Fatigue Crack Resistance of Aluminum Alloy - Alumina Particulate Composites

L. Collini, A. Pirondi and G. Nicoletto

Dept. of Industrial Engineering - University of Parma
Parco Area delle Scienze, 181/A - 43100 Parma

e-mail: collini@me.unipr.it, pirondia@me.unipr.it, nick@me.unipr.it

ABSTRACT. In this work, the fatigue crack growth behaviour of an aluminum alloy (6061-T6) reinforced with alumina (Al_2O_3) particles is characterized. Tests are conducted in Stage I (near-threshold growth rates) and Stage II (Paris regime) at two different R-ratios. Both LT and TL crack orientations are considered. The increase of FCG rates with R-ratio has been interpreted in terms of crack closure for which, in PMMCs contributions from crack surface roughness, crack deflection or trapping mechanisms play an important role. The specimen halves are examined at the SEM after fracture in order to highlight crack path features.

INTRODUCTION

Metal-Matrix Composites (MMCs) are being increasingly considered for several applications in the automotive field (brake discs and drums, brake callipers, pistons), in the railway field (brake discs, callipers and shoes), in sporting goods (bicycle frames, golf clubs and rods), in the aeronautical (reinforced Ti-alloys) and electronic industries (device substrates, packaging) [1]. The interest in particle-reinforced Metal Matrix Composites (PMMCs) mainly stems from their lower cost with respect with short or long fibre-reinforced MMCs [1]. In PMMCs, Al- or Mg-alloys are normally the matrix material while high modulus, particulate ceramics such as Al_2O_3 and SiC are the most common reinforcement materials. The main improvements they offer with respect to the unreinforced alloy are higher stiffness, mechanical and wear resistance [1, 2]. Moreover, a quasi-isotropic mechanical response can be obtained.

In addition to the standard mechanical properties such as tensile or fatigue strength, the knowledge of Fatigue Crack Growth (FCG) properties is also important to guarantee reliable in-service durability. In the case of components subjected to several millions of loading cycles during their expected lifetime (for example, automotive pistons), the behaviour at low FCG rates is of special interest. In this regime, PMMCs show a better performance than unreinforced alloys due to particle-activated shielding mechanisms such as crack deflection or trapping, [3-9]. Furthermore, in cast PMMCs the particles are often located at the grain boundary, leading to a crack tip shielding mechanism known as "egg-shell" [10].

A major influence on FCG properties comes from the R-ratio $R = K_{min}/K_{max}$, where K_{min} and K_{max} are the minimum and maximum values of the applied Stress Intensity Factor (SIF) K, respectively. As in the unreinforced alloy, high R-ratios lead to higher FCG rates with respect to low R-ratios (see for example, [4, 11]). This has been interpreted in terms of crack closure [4], which occurs in PMMCs due to crack surface roughness induced by particles or crack bridging, besides plastic wake contribution that is present also in the unreinforced material.

The aim of this work is to analyse the fatigue crack growth behaviour of an aluminium alloy (6061) reinforced with alumina particles (Al_2O_3), focusing on the influence of R and on crack path features.

METODOLOGIES

Material

The composite under test is a 6061 aluminum alloy with 20% vol. of Al_2O_3 particles incorporated by compocasting. The mix is then extruded and aged to obtain a bar of $100 \times 7 mm^2$ cross-section in a T6 state. The tensile mechanical properties given by the manufacturer are reported in Tab. 1. The fracture toughness measured in a previous work [12] is reported instead in Tab. 2.

Table 1. Tensile mechanical properties of the composite.

Young's modulus E (GPa)	Yield strength R_s (MPa)	Tensile strength R_m (MPa)	Elongation $A_\%$
97	360	375	4

Table 2. Fracture toughness of the composite [12].

Direction	K_{IC} (MPa$\sqrt{m}$)
LT	16.21
TL	15.38

The micrograph of Fig. 1 shows the high uniformity of particle distribution, where only a few isolated large particles and clusters are present. The particle size distribution has been analysed with the help of a commercial software. The results are summarized in the diagram of Fig. 2, from which it comes thet the majority have an area-equivalent diamater D_C of less than 3 microns.
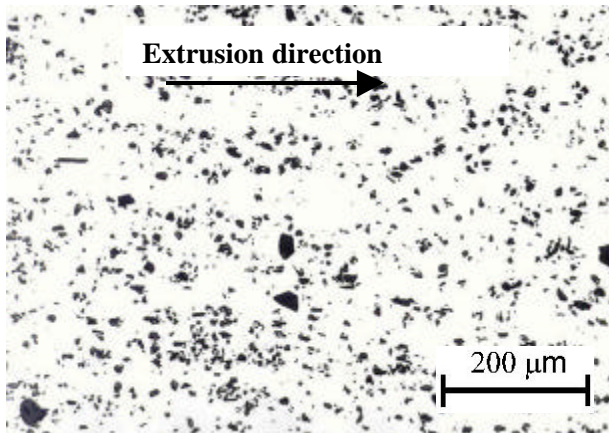
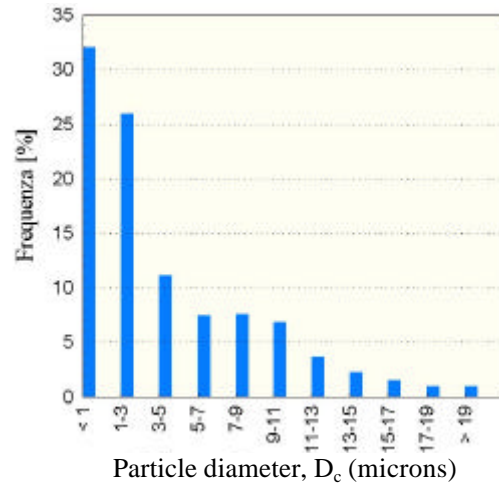Figure 1. Particle distribution, 100x magn.   Figure 2. Particle size distribution.

Specimen and Crack Length Monitoring

A CT specimen geometry with a length $W = 24$mm and thickness $B = 7$mm was adopted in order to optimise the use of the available material (Fig. 3). The applied load was controlled by means of 3000N load cell in order to ensure adequate sensitivity and precision.
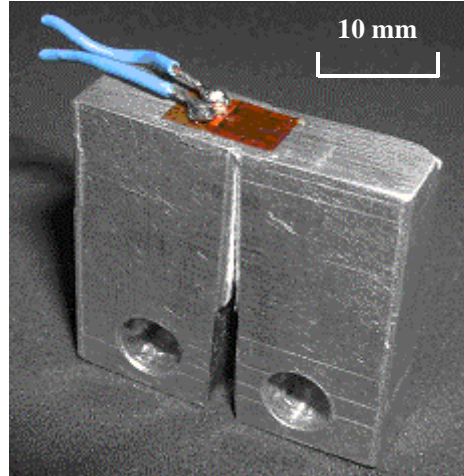

Figure 3. CT specimen adopted in this work.

Since the small dimensions of the specimen did not allow to mount the standard clip-gage for COD measurement, the crack length was monitored during the test with the back-face-strain-gage (BFSG) technique. In this technique, a strain gage is glued to the back face of the specimen, as shown in Fig. 3, and a compliance-like value, C, can be determined from the back-face strain (e) vs load (P) data:

$$C = \frac{-eW}{P} \tag{1}$$

The crack length ratio a/W is obtained from the polynomial relationship:

$$\frac{a}{W} = a_0 + a_1u + a_2u^2 + a_3u^3 + a_4u^4 + a_5u^5 \tag{2}$$

where

$$u = \frac{1}{1+\sqrt{BEC}} \tag{3}$$

The coefficients $a_0,\ ...,\ a_5$ were calibrated by Finite Element Analysis (FEA) and the results are in good agreement with previous results obtained with the surface replication technique, with influence function method and from the literature [13] (see Fig. 4).
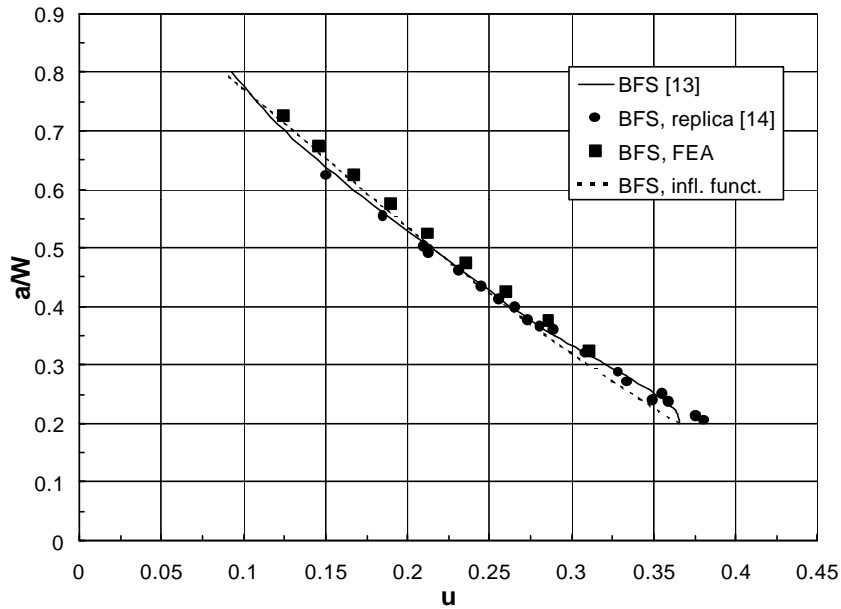

Figure 4. Calibration of a/W as a function of u.

Test Method

The fatigue crack growth tests were conducted at a loading frequency of 10 Hz in lab air. Constant load amplitude and continuous load-shedding procedures depending on the FCG rate range of interest were used. In constant load amplitude tests the applied cyclic load range (i.e. $\mathbf{\Delta}P=P_{max}-P_{min}$) was kept constant throughout the test, while in the continuous load-shedding tests the load range was gradually decreased as the crack propagated according to [15]. As R-ratio dependence is expected to occur also in this class of materials, two load ratios $R=P_{min}/P_{max}$ (0.1 and 0.5, respectively) were

investigated. Both LT and TL crack orientations are considered. The FCG data are presented in log-log (da/dN vs. ΔK) plots. Crack propagation velocities were calculated by the secant method [15].

Evaluation of ΔK_{th}

The threshold stress intensity range was evaluated according to [15], that is a threshold is assumed to be reached when the crack propagation velocity falls below 10^{-7} mm/cycle. In absence of valid data below this limit FCG rate, it is possible to estimate ΔK_{th} by a linear regression in a log-log plot of at least five (da/dN, ΔK) points falling below 10^{-6} mm/cycle.

Since some of the tests did not possess the requirement described above, in those cases the value of ΔK_{th} was estimated using the following procedure:

1. the last portion of the da/dN-ΔK data obtained in ΔK-decreasing tests was approximated with a power law;
2. if points are available below 10^{-6} mm/cycle, the power law approximation is prolonged to intersect the horizontal line at 10^{-7} mm/cycle. The intersection is taken as an estimation of ΔK_{th};
3. if points are not available below 10^{-6} mm/cycle, the procedure described in the previous point is used to find the intersection with an horizontal line at 10^{-6} mm/cycle, taking the corresponding ΔK as a less conservative estimation of ΔK_{th}.

Crack Closure Analysis

As the bulk of the specimen behaves elastically, the force-back deformation plot should conform to a straight line when crack closure is not active. On the other hand, when closure is active, the straight line becomes a non-linear curve due to the progressive contact between the crack faces while unloading. According to Elber's approach, the following loading phase will see the crack tip to open only when the load reaches the so-called opening load, P_{op}, thus reducing the ΔK effectively applied at the crack tip to a $\Delta K_{eff}=K_{max} - K_{op}$, where K_{op} is the stress intensity factor corresponding to P_{op}. The opening load has been evaluated from the loading cycles recorded during the test at the point where deviation from the linearity occurred.

RESULTS AND DISCUSSION

FCG Rates

The influence of the crack orientation (LT or TL) is examined first. The data presented in the diagram of Fig. 5 are referred to the Stage II regime. As with fracture toughness, the FCG rate is not strongly influenced by crack orientation. In Fig. 5 it is shown that the two TL tests performed at R=0.1 and 0.5 lie within the 95% prediction intervals of the respective LT tests. Therefore, in the following analyses no distinction anymore is made between LT and TL orientations.

Besides, the two prediction interval for tests at *R*=0.1 and at *R*=0.5 practically did not overlap each other, meaning that the influence of R-ratio overcomes significantly the experimental scatter.
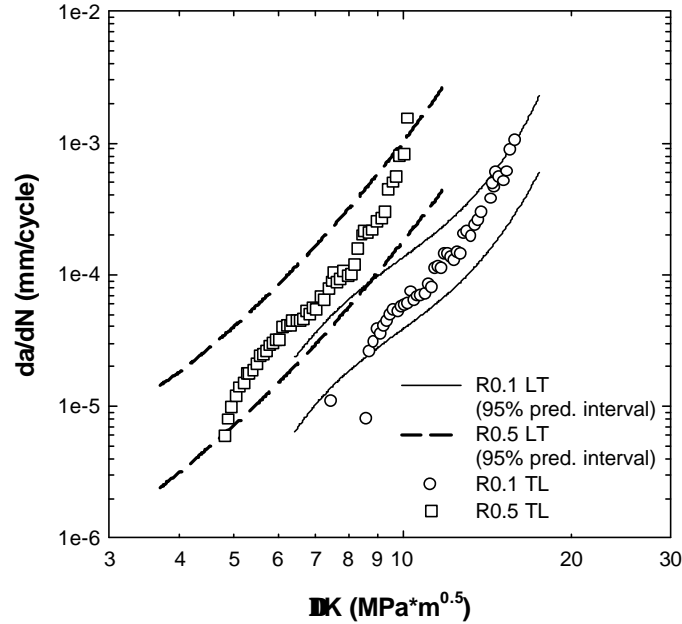

Figure 5. Comparison between TL and LT FCG rates.

The parameters *C* and *m* of the Paris' law $da/dN=C(\Delta K)^m$ were extracted by fitting the experimental data within the range $6*10^{-6}$ to $3*10^{-4}$ mm/cycle of the FCG rates in order to maximize the correlation coefficient. The threshold values were evaluated according to the procedure described previously. The results are summarized in Tab. 3. The exponent m is in line with literature data of SiC- and Al_2O_3-reinforced PMMCs [2, 8] and so does also the estimated ΔK_{th} [4, 8].

Table 3. Parameters of the Paris' law model of FCG behaviour and ΔK_{th} values.

R	*C*	*m*	ΔK_{th} ($MPa\sqrt{m}$)
0.1	$7.88*10^{-9}$	3.97	2.5*
0.5	$1.04*10^{-8}$	4.55	1.4

* estimated at 10-6mm/cycle

The R-ratio does not affect much the exponent of the Paris' law, that means a different mechanism of propagation is not activated by a higher mean load. Anyway, the

FCG rates and the ΔK_{th} are both significantly affected by R-ratio. This is attributed to the appearance of crack closure, as detected from the deviation from linearity of the *P-e* plot. The diagram of Fig. 5 is replotted in Fig. 6 using the $\Delta K_{eff}=K_{max} - K_{op}$ calculated from the opening load detected by the test control software. The prediction intervals of tests at *R*=0.1 and *R*=0.5 overlap on most of the range of ΔK_{eff}, although the two slopes are now quite different from each other.
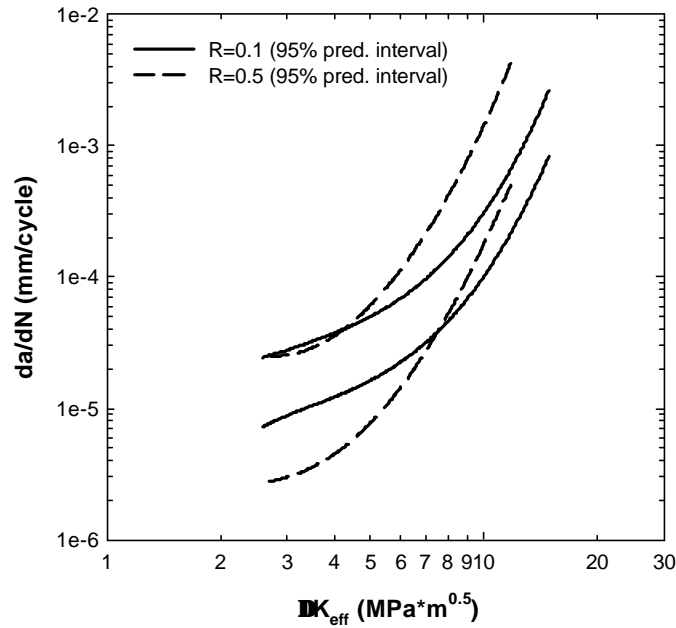

Figure 6. Stage II FCG rates as a function of $\Delta K_{eff}=K_{max} - K_{op}$.

Crack Paths

The fatigue crack paths were observed at the SEM after test for different loading conditions. At this first stage of the work, the magnification factor was kept quite low in order to catch only the fundamental features. The results are shown in Fig. 7a-c in the special case of Stage II crack propagation in a LT specimen tested at R=0.1.

The crack shows deflections from the macroscopic direction of propagation. The crack deflection, which may be originated and enhanced in this material by crack-particle interaction, generates local mixed-mode loading conditions along the crack front that, in turn, dissipate the energy available for Mode I propagation. Besides, crack deflection promotes roughness-induced crack closure.

It is interesting to observe that crack deflection is qualitatively of two different types: i) "short" deflections, whose length is comparable to the particle dimension and, ii) "long" deflections, whose extension is many times the particle size. A slight tilting of observation direction in the SEM allowed to detect this particular morphology also inside the specimen (see Fig. 7). This mechanism seems not to be noticeably influenced by the level of the applied ΔK.
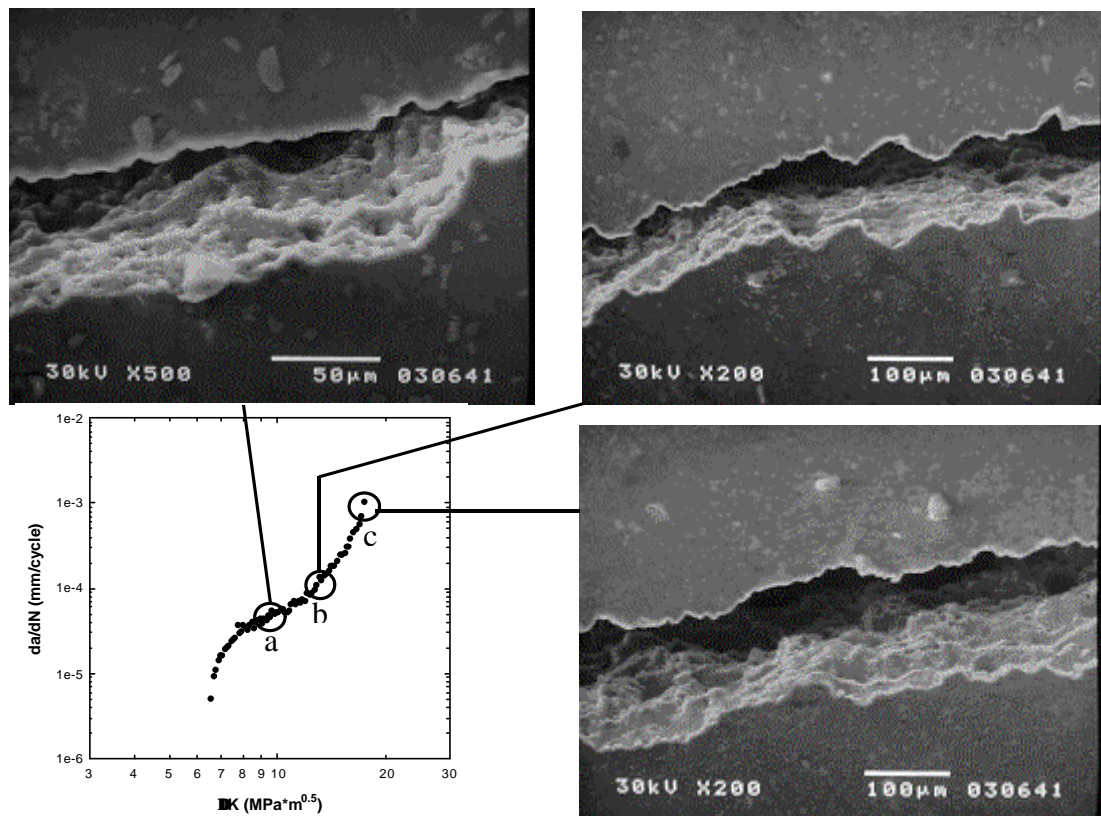
Figure 7a-c. Stage II crack growth path of a test at R=0.1 (LT direction).

CONCLUSIONS

In this work, the fatigue crack growth behaviour of a 6061-T6 aluminum alloy reinforced with alumina particles was characterized. The main conclusions are:
- the properties along LT and TL directions are not significantly different;
- the FCG properties are within the typical range of these materials;
- the influence of R-ratio is significant and can be described using crack closure arguments;
- the crack path shows marked deflections that imply the development of crack shielding mechanisms.

REFERENCES

1. Curran, G. (Jan. 1998) *Materials World*, 20-21.
2. Clyne, T.W. and Withers, P.J. (1995) *An Introduction to Metal Matrix Composites,* Cambridge University Press, Cambridge, UK.
3. Shang, J.K. and Ritchie, R.O. (1989) *Acta Metall et Materialia* **37**, 2267-2278.

4. Lodgson, W.A. and Liaw, P.K. (1986) *Eng Fract Mech* **24**, 737-751.
5. Watt, D.F., Xu, X.Q. and Lloyd, D.J. (1996) *Acta Materialia* **44**, 789-799.
6. Shang J.K., Yu, W. and Ritchie, R.O. (1988) *Mat. Sci. & Eng.* **A102**, 181-192.
7. Davidson, D.L. (1989) In: *ICF 7: Procs 7th Int Conf Fract*, pp. 3021-3028, Salama, K. et al (Eds.).
8. Papakyriacou, M., Mayer, H.R., Tschegg-Stanzl, S.E. and Groschl, M. (1995) *Fat Fract Eng Mat Struct* **18**, 477-487.
9. Liu, G., Shang, J.K. (1996) *Acta Materialia* **44**, 79-91.
10. Wang, Z. (1995). In *Key Engineering Materials* **104-107**, pp. 765-790, Trans Tech Publications, Switzerland.
11. Kumai S., King, E.J. and Knott, J.F. (1990) *Fat Fract Eng Mat Struct* **13**, 477-487.
12. Collini, L. and Pirondi, A. (2002). In: *Proc XXXI AIAS Nat Conf*, Nicoletto, G. et al. (Eds.), Tipografia Benedettina, Parma, Italy.
13. Shaw, W.J.D. and Zhao, W. (1994) *JTEVA* **22**, 512-516.
14. Nicoletto, G. and Pirondi, A. (1997) *Materialove inzinierstvo - Materials engineering Journal*, **4**, Zilina University, Slovak Republic, 10-16.
15. ASTM E647-96. *Annual Book of ASTM Standards - Vol. 3.01*, ASTM, USA.